Available online at www.sciencedirect.com

ScienceDirect

Proceedings of the Combustion Institute 35 (2015) 1887–1894

Proceedings of the Combustion Institute

www.elsevier.com/locate/proci

Kinetics of nascent soot oxidation by molecular oxygen in a flow reactor

Joaquin Camacho, Yujie Tao, Hai Wang *

Mechanical Engineering Department, Stanford University, Stanford, CA 94305-3032, USA

Available online 24 June 2014

Abstract

Oxidation kinetics of soot is typically measured with well aged soot as substrates. Recent studies show that nascent soot can have structures and surface composition drastically different from mature, graphitized soot. In the present study, the kinetics of nascent soot oxidation by molecular oxygen was observed at temperatures of 950, 1000 and 1050 K for molecular oxygen concentrations ranging from 1000 to 7800 ppm at ambient pressure in a coupled burner-stabilized stagnation flame burner and laminar aerosol flow reactor. The reactant particles, 10–20 nm in diameter, were freshly synthesized from premixed flames of ethylene, *n*-heptane, and toluene and introduced into the flow reactor continuously. The kinetics of particle oxidation was measured through electric mobility measurement of particle size distributions before and after oxidation. It was found that the specific oxidation rate is has a first-order dependency on gas-phase O_2 concentration over the range of O_2 concentration studied. The rate measured is an order of magnitude larger than that predicted by the classical Nagle Strickland-Constable (NSC) correlation. The result suggests that the surface of nascent soot is considerably more reactive towards oxidation than graphite or graphitized soot.

Keywords: Soot; Particle size distribution; Kinetics; Oxidation; Reactivity

1. Introduction

Recent studies suggest that soot can exhibit structural and chemical compositional complexities that have not been fully understood [1–3]. Soot microstructure varies with flame chemistry and conditions [4–6]. Nascent soot is known to contain amorphous components and mixtures of sp^2 and sp^3 carbon [7–9] and can exhibit little ordering of graphitic planes [10]. Mixed sp^2/sp^3 phases have also been observed in mature soot [11,12]. Additionally, nascent and mature soot show differences in details of interior and surface microstructures [4,13–15]. Because the heterogeneous reaction kinetics and mechanisms are expected to be sensitive to surface structure and composition, the oxidation kinetics of nascent soot surfaces is not expected to be the same as that of aged or graphitized carbon surfaces. Similarly, the rate of nascent soot oxidation by molecular oxygen can be substantially different from what

* Corresponding author. Address: Mechanical Engineering Department, Stanford University, 452 Escondido Mall, Stanford, CA 94305-3032, USA. Fax: +1 650 723 1748.

E-mail address: haiwang@stanford.edu (H. Wang).

http://dx.doi.org/10.1016/j.proci.2014.05.095
1540-7489/

is described by the classical Nagle-Strickland Constable (NSC) equation [16] derived for graphite or carbon black.

Theory of carbon oxidation by O_2 was first proposed by Eyring and coworkers [17]. Two distinct reaction sites were introduced to explain the maxima observed in the oxidation rate and this was also considered in the NSC expression from observations of bulk pyrographite oxidation [16]. The NSC expression has since been extended to high-temperature soot oxidation [18,19]. The rates predicted by the NSC expression were found to be in good agreement under a certain flame condition with rates derived from gas-phase analogous reactions of phenyl + O_2 [20].

A wide range of experimental techniques has been used to probe carbon particle oxidation by O_2. The oxidation rate has been determined at temperatures above 1700 K by aerosolizing carbon black in shock tubes [21–24]. Soot oxidation has also been studied in flame/dual flame environments or vitiated oxidizing flows [4,25–29], in some cases, using soot freshly prepared in flames [30,31]. Soot synthesized in a pyrolysis flow reactor was shown to be more reactive towards oxidation than that predicted by the NSC expression; and the reactivity appears to be sensitive to the source fuel from which soot is synthesized [4].

The oxidation of soot has also been studied *ex situ*. For example, gravimetric analysis has been applied to carbon black, flame soot and diesel soot exposed to an oxidant in immobilized beds [32–39] over wide ranges of temperature, oxidant concentration and particle size. The oxidation of flame and diesel soot has also been followed by transmission electron microscopic analysis of particle size and morphology [40–42]. The Tandem Differential Mobility Analyzer method has been introduced and used by Zachariah and coworkers (e.g., [43–46]) to examine the oxidation of soot at the tip of a coflow diffusion flame and from a diesel engine. A comparable study on nascent soot during the early stage of its growth has not been attempted, and there are no direct kinetic observations made for the oxidation of nascent soot by O_2 under well-defined conditions.

In the present work, the rate of nascent soot oxidation by O_2 was examined at around 1000 K over a range of oxygen concentration in an aerosol flow reactor. The various obstacles to measuring the oxidation kinetics of nascent soot were minimized by using fresh soot extracted simultaneously and continuously from a burner-stabilized stagnation (BSS) flame as the soot reactant. To understand the potential effect of fuel structure towards oxidation reactivity of flame soot, three different flames were used to generate soot using ethylene, *n*-heptane and toluene as the parent fuels. The results are compared between the different fuels and against the predictions made by the NSC expression.

2. Experimental

In developing the experimental setup, our emphasis was placed on minimizing the transit time from the point where soot was extracted from a flame to the flow reactor inlet. The short transit time and suspension of reactant particles within an inert flow minimizes the change in the surface composition. Like the work of Zachariah and coworkers [43–46], we utilized electric mobility as the primary diagnostic. Unlike their work, the reactant particles examined here are younger and have not undergone considerable carbonization. A schematic summarizing the experimental setup is shown in Fig. 1. There are three key elements: (1) a BSS flame that produces the fresh nascent soot, (2) a flow reactor that oxidizes the soot in a flow containing O_2 diluted in N_2, and (3) a particle sizer that measures the particle size distributions before and after the oxidation occurs. All components are operated at the ambient pressure or close to the ambient pressure.

The BSS flame is composed of a flat flame burner and a water-cooled stagnation surface that is also used for particle sampling. The flame setup has a pseudo one-dimensional flow with well-defined boundary conditions [47]. It allows for the temperature–stoichiometry–time history of soot to be controlled to an extent and the size distribution probed at the different stages of soot growth. The flat flame burner is 5 cm in diameter and is uncooled. A sheath of nitrogen shields the flame to prevent radial entrainment and diffusion of oxygen from ambient air. Nascent soot was extracted at a distance of 0.8 cm from the burner surface using a stagnation-surface probe—a method similar to our earlier characterization of particle size distribution function (PSDF) in BSS flames [47–49].

Nascent soot entering into the orifice in the stagnation-surface probe was immediately diluted and chilled in a flow of cold nitrogen. The dilution ratio is approximately 100. The aerosol was carried to the flow reactor within a transmission time of 0.1 s and mixed with a preheated stream of oxygen/nitrogen or nitrogen that enters into a tubular flow reactor of 1.8 cm inner diameter. The temperature of the flow reactor was monitored at the reactor inlet, the reactor outlet and at one point within the heated length. The temperatures measured at the three positions are roughly equal with the standard deviation of 3 K. Oxidation of nascent soot was observed at $T = 950$, 1000 and 1050 K for oxygen concentrations ranging from 1000 to 7800 ppm. The highest O_2 concentration was chosen because of experimental hardware limitations. The total flow rate in the test section of the flow reactor was kept at 330 cm^3/s (298 K and 1 atm) for every oxygen concentration. The residence times ranges from 0.20 to 0.22 s depending on the reactor temperature. The Reynolds

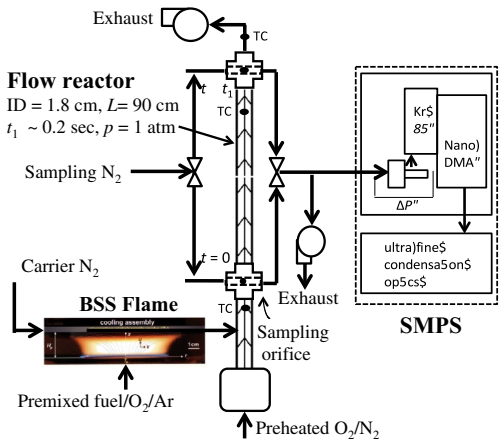

Fig. 1. Schematic of the experimental apparatus.

number in the reactor is 700 under these conditions.

The diagnostic for nascent soot oxidation is the change in the PSDF, which was measured with a TSI Scanning Mobility Particle Sizer (Electrostatic Classifier 3085 and Condensation Particle Counter 3025). Sampling probes embedded at the inlet and outlet of the aerosol reactor allowed for the PSDF to be measured before and after oxidation.

Three flames generated different soot reactants. The flame compositions and properties are summarized in Table 1. The mass-flow rates were controlled by critical orifices for all gaseous flows into the BSS flame and flow reactor. A syringe pump meters the flow rate of liquid fuels. The fuel was injected into a vaporizer through a microspray and mixed with a pre-heated flow of oxygen and argon.

3. Data analysis

For a particle of an arbitrary shape, the mass disappearance rate due to surface oxidation is:

$$\frac{dm}{dt} = \omega S, \tag{1}$$

where m is the particle mass, t the time, S is the surface area, and ω the specific surface oxidation rate (g/cm^2 s). If the mass density ρ_s is constant and fragmentation is negligible, the specific oxidation rate, ω, may be given by

$$\omega = -\frac{\rho_s}{2}\frac{d\chi}{dt} \tag{2}$$

as long as a suitable size parameter χ can be defined. In the case of a sphere, the obvious choice for χ is the diameter; and for a rounded cylinder or a spheroid, χ may be taken as the diameter of the cylinder and the circle on the major-axis plane.

As will be shown later, all of the PSDFs to be treated here are lognormal or close to lognormal, in which case the median mobility diameter $\langle D_p \rangle$ of such a PSDF may be chosen as the characteristic size parameter χ. To the first approximation, we have $\omega \cong -(\rho_s/2)(\Delta\langle D_p\rangle/\Delta t)$. This simplest method of analysis is referred to as Model I hereafter. A more appropriate way to analyze the data involves a full PSDF modeling, in which case the time rate of change of the mobility diameter is a constant and the number concentration is conserved. This is the second model (Model II) employed in our analysis, in which the specific oxidation rate was obtained through a least squares fitting of the measured PSDFs. Though they are simple to implement, the above models cannot reproduce the measured PSDF when a substantial size change occurs. A possible cause is the spherical-shape assumption in the interpretation of mobility diameter. In fact, recent studies of nascent soot by Helium Ion Microscopy [50,51] showed that (a) nascent soot as small as 10 nm can exhibit elongated shapes due to aggregation, and (b) these aggregates can have a quite large aspect ratio. A third model (Model III) was thus employed in which the PSDFs are described by the sum of two lognormal distributions. The first size mode characterizes small, spherical particles, and the second mode measures larger particles and have shapes that can be a rounded cylinder or prolate spheroidal. Because non-spherical shapes of real soot particles must be interpreted in a statistical manner (i.e., each particle has its own shape and there is no two particles that are identical), some idealization must be considered here. A rounded cylinder of diameter D and length between the two half-sphere centers equal to L was chosen as our model system. It turns out that the exact shape does not impact the

Table 1
Summary of flame conditions for the BSS flame soot.

	Mole fraction[a]		ϕ	Velocity[b], v_0 (cm/s)	Temperature, $T_{f,max}$ (K)
	Fuel	O_2			
Ethylene	0.1510	0.218	2.07	10.55	1915
n-Heptane	0.0427	0.227	2.07	7.47	1900
Toluene	0.0326	0.169	1.77	9.28	2035

[a] The balance gas is argon.
[b] 298 K and 1 atm.

calculation of the ω value notably, as will be discussed later. Thus we find that $\chi = D$ and the mobility area to be the mean, two-dimensional projection of the rounded cylinder, $S_c = \pi D^2/4 + \sqrt{2}DL/2$. The spherical equivalent mobility diameter D_p is given by the relationship

$$D_p^2 = D^2 + 2\sqrt{2}DL/\pi \quad (3)$$

The oxygen is in excess within its concentration range employed in comparison with reactant particle surface loading. Therefore the oxidation reaction occurs in the pseudo first-order regime with respect to the particle surface. The soot particle density in the current work, ρ_s, was taken to be 1.5 g/cm^3 based on earlier work conducted on similar flames [52].

4. Results and discussion

Particle–particle coagulation and decomposition must be suppressed in the flow reactor for the shift in PSDF to an effective indication of oxidation. The normalized PSDF under inert nitrogen condition, comparing measurements made at the inlet (0 s) and outlet (~0.2 s) of the flow reactor is shown in Fig. 2. As can be seen, there is no observable change in the PSDF over the reaction time, indicating that the effect of these processes was minimal. The observation is consistent with the total number density of the reactant soot chosen in the experiment. At $N = 10^7$ cm^{-3} total number density, the time scale for particle–particle coagulation to be observable is around 1 min. Additionally, the mean free path of the gas is larger than the size of the particles studied therefore no mass transfer limitations are expected. Figure 2 also shows that $\langle D_p \rangle = 11$, 13 and 18 nm for soot reactants made from the ethylene, *n*-heptane and toluene flame, respectively. The broader distribution of the particle size observed for the toluene flame is related to the stability of that flame, causing soot production to fluctuate somewhat and leading to PSDF broadening.

Oxidation behavior for a range of oxygen concentrations was measured at flow reactor temperatures of 957 ± 2, 1014 ± 2 and 1050 K. PSDF data are shown in Fig. 3 for soot reactant produced in the *n*-heptane flame at reactor temperature of 1017 K. The PSDFs and their variations for reactant particles produced from the ethylene, *n*-heptane and toluene flames for all reactor conditions can be found in the Supplemental material. For each condition, the experiments were repeated at least three times to ensure reproducibility. Shifts in the particle diameter were observable for O_2 concentration >1000 ppm at 950 K and the shift is more dramatic for increased O_2 concentration or temperature. As shown in Fig. 3, most of the particle mass is consumed before the

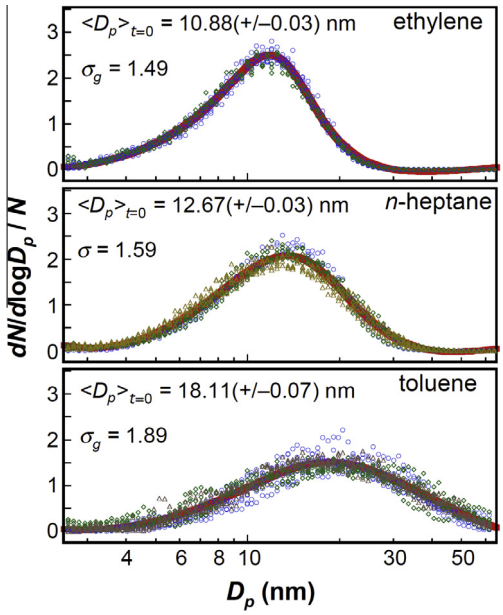

Fig. 2. Normalized PSDFs of soot from the ethylene, *n*-heptane and toluene flames probed at the inlet of the flow reactor ($t = 0$ s; lines) and at the exit in an N_2 flow for temperature and time of 950 K and 0.22 s (circles), 1000 K and 0.21 s (diamonds) and 1050 K and 0.20 s (triangles). The total number density N is around 10^7 #/cc.

oxygen concentration reaches 1% (mol). This extent of particle conversion is similar for every fuel and most conditions studied as shown in the Supplementary material.

A comparison of the three models is also shown in Fig. 3 in terms of the fit to the PSDFs for *n*-heptane-flame soot at reactor temperature of 1017 K. The diameter shown is the mobility diameter that measures the average two-dimensional projection area rather than the actual diameter. The results of Models I and II are demonstrated in the left column and those of Model III are presented in the right column for the same conditions. For 1000 ppm O_2 concentration, all three models reproduce the measured PSDF but the agreement of Models I and II weakens as oxygen concentration is increased. The cause is clearly in the broadening of the simulated PSDF resulting from the large particles not losing mass as fast as observed. Overall, the failure of the two models lies in the spherical-shape assumption in the interpretation of the mobility diameter. The discrepancy between experiment and model is an indication that the spherical-shape assumption under-estimates the particle surface area available for oxidation.

To illustrate what was just discussed, we introduce Model III in which the size distribution is decomposed into two separate lognormal functions, one describing small, spherical particles

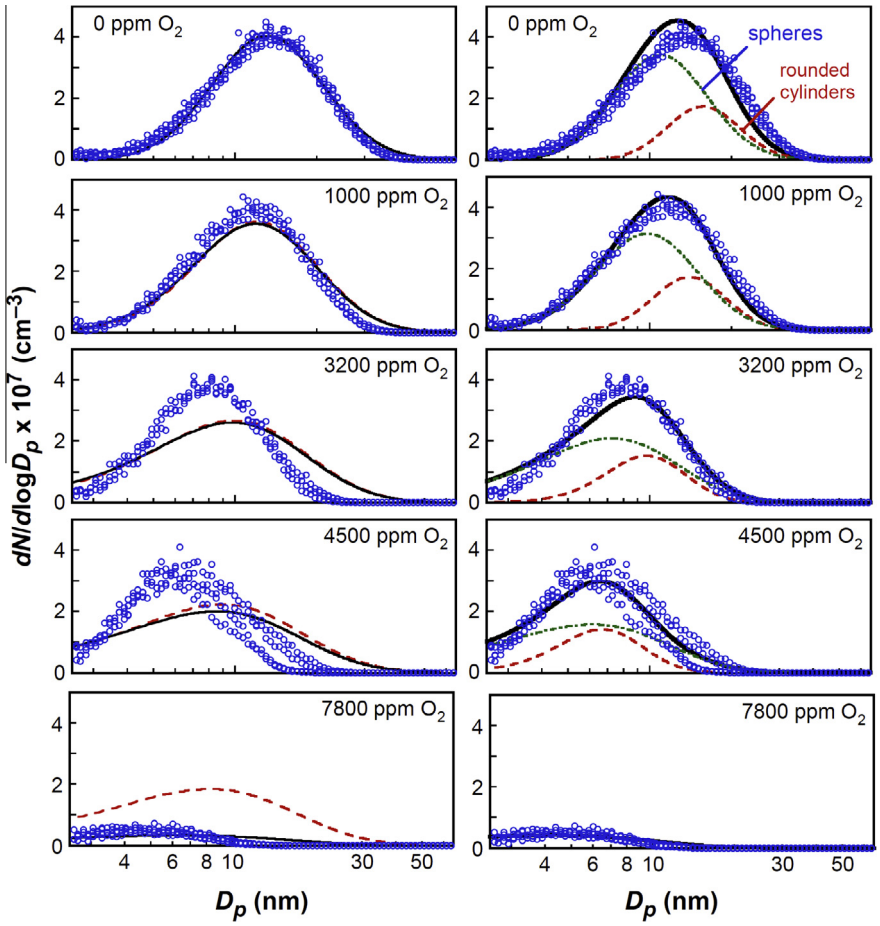

Fig. 3. PSDFs (symbols) measured for nascent soot oxidation at 1017 K after 0.203 s of reaction time in the flow reactor. The reactant soot is produced from the *n*-heptane flame. Left panel: fits to data using Models I (dashed line) and II (solid line); right panel: fits to data using Model III (solid line).

and the other representing rounded cylinders of different length L. As shown in Fig. 3, this variation in particle shape assumptions allows for an adequate description of the entire distribution function for all oxygen concentrations. The results shown are joint fits to the PSDF data with respect to the initial cylinder diameter D of the unreacted soot and ω value for a specific oxygen concentration. In all cases, the best fit yields a D value of 8 nm for the case shown in Fig. 3. For ethylene- and toluene-flame soot, the best D values are 8 and 13 nm, respectively, which are well within the range observed earlier [51,52]. The ratio of the number density ratio of the spherical particles to rounded cylinders was found to be about 2 to 1, as shown in the right column of Fig. 3. Clearly, rounded cylinders provide greater surface areas and are oxidized faster than spherical particles. Other models have been considered during the course of data analysis. These include variable mass density of the particle material, particle fragmentation and diffusion limited processes, but none yielded results as convincing as Model III. For example, an internal reaction formulation is analyzed in the Supplemental material. Also, there are no features in the measured PSDFs that are indicative of fragmentation over the range of temperature tested.

Interestingly, the ω values extracted from the three models are similar at in the low range of O_2 concentrations. For comparison, we present in Fig. 4 the ω values for the heptane-flame soot as a function of oxygen concentration. For $[O_2] < 6 \times 10^{-8}$ mol/cm^3, the ω values obtained from the three models overlap with each other and exhibits a first-order dependency on O_2 concentration. The ω values diverge only for the highest O_2 concentration measured. Only Model III yields the expected first-order behavior over the entire range of O_2 concentration.

The first order dependency on $[O_2]$ is verified for soot reactants from all flames under the

conditions tested. Figure 5 shows the variation of ω as a function of $[O_2]$ for all flame soot and reactor temperatures studied. The intrinsic rate constant (g cm/mol s) is taken as the slope of the ω-versus-$[O_2]$ plot, i.e., $k = \omega/[O_2]$. Figure 6 presents an Arrhenius plot for the intrinsic rate constant, which is found to be independent of the soot reactants produced from the three flames. The apparent activation energy was found to be 21.4 ± 3.7 kcal/mol.

For nascent soot studied herein, we found that the specific oxidation rate is an order of magnitude greater than what is predicted by the NSC equation over the temperature range studied. This comparison is shown in Fig. 7; and this result is expected considering that nascent soot should be more reactive than graphite or carbonized soot from which the NSC equation was developed. Previously, Vander Wal and Tomasek [4] examined soot burnout rates by directly injecting newly formed particles from a pyrolysis flow reaction into the post-flame region of a lean flame. Similar to the current study, the burnout rates reported were shown to be more than an order of magnitude faster than NSC.

There are differences in results obtained here and those in the literature. It has been reported [39] that the reactivity of soot produced in *n*-heptane and ethylene diffusion flames is inversely proportional to the age of the soot in the flame. Ethylene-flame derived soot was found to be less reactive than *n*-heptane soot because the ethylene flame produced soot earlier. The lack of sensitivity towards the parent fuel observed currently is probably due to the fact that the soot reactants were sampled with a comparable aging process

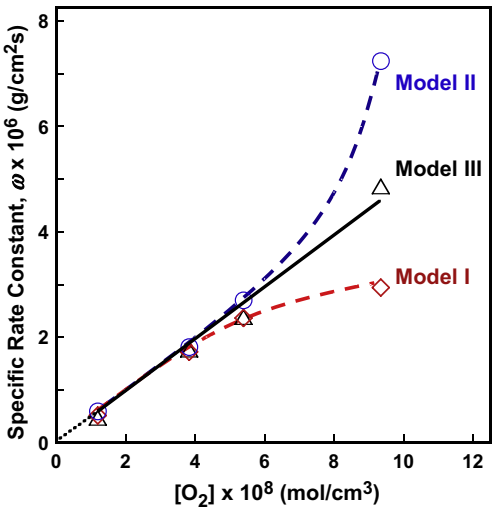

Fig. 4. Specific rate constant, ω, of heptane-flame soot at 1017 K, 0.203 s reaction time as a function of O_2 concentration comparing the three models.

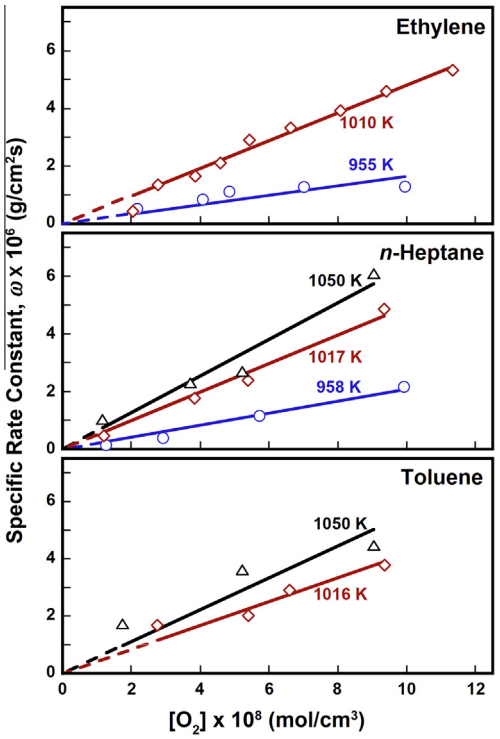

Fig. 5. Specific rate constant ω as a function of O_2 concentration for reactant soot generated from the ethylene, *n*-heptane and toluene flames.

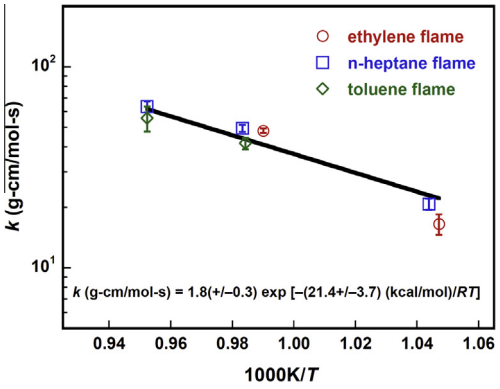

Fig. 6. Arrhenius plot of the intrinsic rate constant k for all reactant soot over the temperature range measured.

across the flames studied. In another study, soot formed in a pyrolysis flow reactor was entrained in the post-flame region of an oxygen-rich flame [4]. Benzene soot was shown to be more reactive towards oxidation than the ethylene soot. The variation in reactivity may also be indicative of the fact that the soot microstructure is a strong function of the local condition (temperature, residence time, hydrogen content, etc.) under which

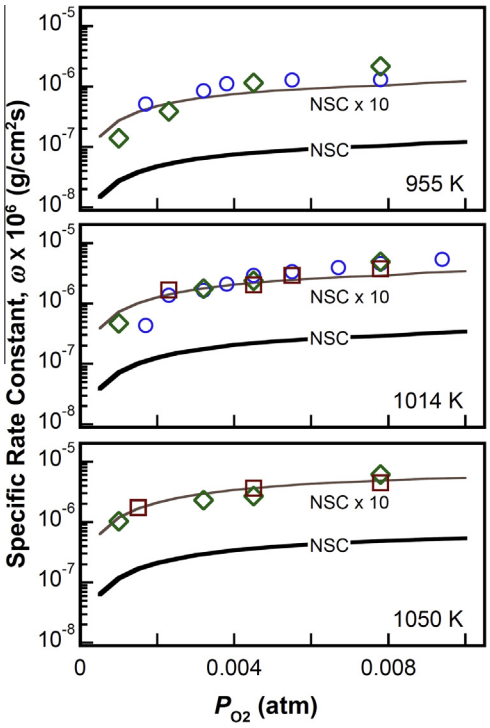

Fig. 7. Specific oxidation rates measured for nascent soot produced from ethylene (circles), *n*-heptane (diamonds) and toluene (squares) flames and compared to predictions by the NSC equation (solid lines).

soot forms and grows, and of course, local conditions of the flame is impacted by the fuel composition. Other studies [23,25,43] reported kinetic rates of soot or carbon black particle oxidation by O_2 that are generally in line with the NSC expression. The cause for the difference is no other than the fact that soot is not a uniquely defined material, and as such the surface reaction mechanisms must vary as a function of the composition. For example, Higgins et al. [43] reported the oxidation rate of carbonized soot sampled from the tip of a co-flow diffusion flame to be consistent with the NSC expression, and this soot is more carbonized than the nascent soot studied herein.

5. Conclusions

Kinetics of soot oxidation by molecular oxygen was observed under the ambient pressure for nascent soot particles during early stages of mass and size growth in a novel flow reactor coupled with a burner-stabilized stagnation flame burner. Nascent soot was generated in ethylene, *n*-heptane and toluene flames and immediately introduced in the flow reactor as an aerosol. The rate of change in the median particle diameter due to oxidation was measured to be O(10 nm/s) at around 1000 K and a few thousand PPM of O_2. The specific rate of oxidation was observed to have a first-order dependency on gas-phase O_2 concentration over the range of O_2 concentration studied. The rate is about an order of magnitude greater than that predicted by the NSC equation, which suggests that the surface of nascent soot is more reactive than graphite or carbonized soot surfaces.

Acknowledgements

Work was supported Reaction Design Model Fuels Consortium II (JC) and by the Combustion Energy Frontier Research Center (CEFRC) (YT & HW), an Energy Frontier Research Center funded by the U.S. Department of Energy, Office of Science, Office of Basic Energy Sciences under Award Number DE-SC000119.

Appendix A. Supplementary data

Supplementary data associated with this article can be found, in the online version, at http://dx.doi.org/10.1016/j.proci.2014.05.095.

References

[1] A. D'Anna, *Proc. Combust. Inst.* 32 (2009) 593–613.
[2] H. Wang, *Proc. Combust. Inst.* 33 (2011) 41–67.
[3] R.L. Vander Wal, V.M. Bryg, M.D. Hays, *Aerosol Sci.* 41 (2010) 108–117.
[4] R.L. Vander Wal, A.J. Tomasek, *Combust. Flame* 134 (2003) 1–9.
[5] R.L. Vander Wal, A. Strzelec, T.J. Toops, C.S. Daw, C.L. Genzale, *Fuel* 113 (2013) 522–526.
[6] C. Han, Y. Liu, J. Ma, H. He, *J. Chem. Phys.* 137 (2012) 084507.
[7] B. Öktem, M.P. Tolocka, B. Zhao, H. Wang, M.V. Johnston, *Combust. Flame* 142 (2005) 364–373.
[8] J.P. Cain, P.L. Gassman, H. Wang, A. Laskin, *Phys. Chem. Chem. Phys.* 12 (2010) 5206–5218.
[9] J.P. Cain, J. Camacho, D.J. Phares, H. Wang, A. Laskin, *Proc. Combust. Inst.* 33 (2011) 533–540.
[10] P. Minutolo, G. Rusciano, L.A. Sgro, G. Pesce, A. Sasso, A. D'Anna, *Proc. Combust. Inst.* 33 (2011) 649–657.
[11] C.K. Gaddam, R.L. Vander Wal, *Combust. Flame* 160 (2013) 2517–2528.
[12] R.L. Vander Wal, V.M. Bryg, C.-H. Huang, *Combust. Flame* 161 (2014) 602–611.
[13] R.L. Vander Wal, A.J. Tomasek, *Combust. Flame* 136 (2004) 129–140.
[14] R.L. Vander Wal, A. Yezerets, N.W. Currier, D.H. Kim, C.M. Wang, *Carbon* 45 (2007) 70–77.
[15] H.J. Seong, A.L. Boehman, *Combust. Flame* 159 (2012) 1864–1875.
[16] J.R. Walls, R.F. Strickland-Constable, *Carbon* 1 (1964) 333–338.
[17] G. Blyholder, J.S. Binford, H. Eyring, *J. Phys. Chem.* 62 (1958) 263–267.

[18] B.R. Stanmore, J.F. Brilhac, P. Gilot, *Carbon* 39 (2001) 2247–2268.
[19] A.A. Lall, M.R. Zachariah, *Size resolved soot oxidation kinetics*, in: H. Bockhorn, A.F. D'Anna, H. Wang (Eds.), *Combustion Generated Carbonaceous Particles*, KIT Scientific Publishing, 2009.
[20] M. Frenklach, H. Wang, *Proc. Combust. Inst.* 23 (1991) 1559–1566.
[21] C. Park, J.P. Appleton, *Combust. Flame* 20 (1973) 369–379.
[22] O. Brandt, P. Roth, *J. Aerosol Sci.* 19 (1988) 863–866.
[23] O. Brandt, P. Roth, *Combust. Flame* 77 (1989) 69–78.
[24] P. Cadman, R.J. Denning, *J. Chem. Soc. Faraday Trans.* 92 (1996) 4159–4165.
[25] K.B. Lee, M.W. Thring, J.M. Beer, *Combust. Flame* 6 (1962) 137–145.
[26] C.P. Fenimore, G.W. Jones, *J. Phys. Chem.* 71 (1967) 593–597.
[27] A. Feugier, *Combust. Flame* 19 (1972) 249–256.
[28] A. Garo, G. Prado, J. Lahaye, *Combust. Flame* 79 (1990) 226–233.
[29] T. Schafer, F. Mauss, H. Bockhorn, F.Z. Fetting, *Naturforsch., A: Phys. Sci.* 50 (1995) 1009.
[30] C.A. Echavarria, I.C. Jaramillo, A.F. Sarofim, J.S. Lighty, *Proc. Combust. Inst.* 33 (2011) 659–666.
[31] C.A. Echavarria, I.C. Jaramillo, A.F. Sarofim, J.S. Lighty, *Combust. Flame* 159 (2012) 2441–2448.
[32] K. Otto, M.H. Sieg, M. Zinbo, Bartosiewicz, SAE Technol. Pap. Ser No. 800336, 1980.
[33] P. Gilot, F. Bonnefoy, F. Marcuccilli, G. Prado, *Combust. Flame* 95 (1993) 87–100.
[34] J.P.A. Neeft, T.X. Nijhuis, E. Smakman, M. Makkee, J.A. Moulijn, *Fuel* 76 (1997) 1129–1136.
[35] J.M. Encinar, J.F. González, E. Sabio, J.J. Rodríguez, *J. Chem. Technol. Biotech.* 75 (2000) 213–222.
[36] K.O. Lee, H. Seong, S.M. Choi, *Proc. Combust. Inst.* 34 (2011) 3057–3065.
[37] J.H. Song, M. Alam, A.L. Boehman, U. Kim, *Combust. Flame* 146 (2006) 589–604.
[38] K. Al-Qurashi, A.D. Lueking, A.L. Boehman, *Combust. Flame* 158 (2011) 1696–1704.
[39] J.H. Seong, A.L. Boehman, *Combust. Flame* 159 (2012) 1864–1875.
[40] T. Ishiguro, Y. Takatori, K. Akihama, *Combust. Flame* 108 (1997) 231–234.
[41] R.L. Vander Wal, C.J. Mueller, *Energy Fuels* 20 (2006) 2364–2369.
[42] H. Jung, D.B. Kittelson, M.R. Zachariah, *Combust. Flame* 136 (2004) 445–456.
[43] K.J. Higgins, H. Jung, D.B. Kittelson, J.T. Roberts, M.R. Zachariah, *J. Phys. Chem. A* 106 (2001) 96–103.
[44] S.H. Kim, R.A. Fletcher, M.R. Zachariah, *Environ. Sci. Technol.* 39 (2005) 4021–4026.
[45] A.M. Nienow, J.T. Roberts, M.R. Zachariah, *J. Phys. Chem. B* 109 (2005) 5561–5568.
[46] H. Jung, D.B. Kittelson, M.R. Zachariah, *Environ. Sci. Technol.* 40 (2006) 4949–4955.
[47] A.D. Abid, J. Camacho, D.A. Sheen, H. Wang, *Combust. Flame* 156 (2009) 1862–1870.
[48] J. Camacho, S. Lieb, H. Wang, *Proc. Combust. Inst.* 34 (2013) 1853–1860.
[49] A.D. Abid, J. Camacho, D.A. Sheen, H. Wang, *Energy Fuels* 23 (2009) 4286–4294.
[50] M. Schenk, S. Lieb, H. Vieker, A. Beyer, A. Gölzhäuser, H. Wang, K. Kohse-Höinghaus, *ChemPhysChem* 14 (2013) 3248–3254.
[51] M. Schenk, S. Lieb, H. Vieker, A. Beyer, A. Gölzhäuser, H. Wang, K. Kohse-Höinghaus, *Proc. Combust. Inst.* 35 (2) (2015) 1879–1886. http://dx.doi.org/10.1016/j.proci.2014.05.009.
[52] B. Zhao, K. Uchikawa, H. Wang, *Proc. Combust. Inst.* 31 (2007) 851–860.